Front. Phys. 13(2), 137402 (2018)
https://doi.org/10.1007/s11467-017-0728-0

RESEARCH ARTICLE

Topological Fulde–Ferrell and Larkin–Ovchinnikov states in spin-orbit-coupled lattice system

Yao-Wu Guo[1], **Yan Chen**[1,2,†]

[1] *Department of Physics and State Key Laboratory of Surface Physics, Fudan University, Shanghai 200433, China*
[2] *Collaborative Innovation Center of Advanced Microstructures, Nanjing 210093, China*
Corresponding author. E-mail: [†] *yanchen99@fudan.edu.cn*
Received August 27, 2017; accepted September 24, 2017

The spin-orbit coupled lattice system under Zeeman fields provides an ideal platform to realize exotic pairing states. Notable examples range from the topological superfluid/superconducting (tSC) state, which is gapped in the bulk but metallic at the edge, to the Fulde–Ferrell (FF) state (having a phase-modulated order parameter with a uniform amplitude) and the Larkin–Ovchinnikov (LO) state (having a spatially varying order parameter amplitude). Here, we show that the topological FF state with Chern number ($\mathcal{C} = -1$) (tFF_1) and topological LO state with $\mathcal{C} = 2$ (tLO_2) can be stabilized in Rashba spin-orbit coupled lattice systems in the presence of both in-plane and out-of-plane Zeeman fields. Besides the inhomogeneous tSC states, in the presence of a weak in-plane Zeeman field, two topological BCS phases may emerge with $\mathcal{C} = -1$ (tBCS_1) far from half filling and $\mathcal{C} = 2$ (tBCS_2) near half filling. We show intriguing effects such as different spatial profiles of order parameters for FF and LO states, the topological evolution among inhomogeneous tSC states, and different non-trivial Chern numbers for the tFF_1 and $\mathrm{tLO}_{1,2}$ states, which are peculiar to the lattice system. Global phase diagrams for various topological phases are presented for both half-filling and doped cases. The edge states as well as local density of states spectra are calculated for tSC states in a 2D strip.

Keywords topological superfluid, Fulde–Ferrell (FF) state

PACS numbers 74.20.Fg, 74.70.Tx, 03.75.Ss

Topological quantum states of matter have attracted a tremendous amount of attention both theoretically and experimentally during the last decade [1, 2]. In particular, the topological superfluid/superconducting (tSC) state hosts zero-energy edge states usually related to Majorana fermions (MFs), which are their own antiparticles [3, 4]. MFs obey non-Abelian braiding statistics and have potential applications in fault-tolerant topological quantum computation [5]; therefore, probing MFs in solid-state and ultracold-atom systems is a topic of considerable interest [6–10]. At present, a number of exotic quantum systems, such as $\nu = 5/2$ fractional quantum Hall states [11], chiral p-wave superconductors [12, 13], and heterostructures composed of s-wave superconductors and semiconductor nanowires or topological insulators [2, 10, 14–19], are believed to support MFs. Besides these real materials, the experimental realization of spin-orbit coupling (SOC) in cold-atom superfluid systems [20–22] provides an ideal platform to search exotic tSC states. In these systems, the SOC and out-of-plane Zeeman field mix different spin states and split the spin states at the Fermi surface, leading to intra-band and inter-band pairings. If the intra-band pairing is an effective p-wave interaction, the system becomes topologically non-trivial. Recently, much theoretical work has focused on the tSC state in the presence of the out-of-plane Zeeman field [14, 23, 24]. Nonetheless, inhomogeneous superfluid/superconducting states with spontaneously broken translational invariance, known as Fulde–Ferrell (FF) and Larkin–Ovchinnikov (LO) states, are still at the center of interest in many diverse fields of physics [25–28]. Predicted theoretically around 50 years ago [29, 30], both FF and LO states contain a finite number of Cooper pairs with center-of-mass momentum, arising from the interplay between the competing magnetic and SC orders. In particular, the FF state corresponds to a phase-modulated order parameter of uniform amplitude, whereas the LO state has a spatially varying order

*arXiv: 1710.07169.

parameter amplitude. Normally, the LO state has lower energy than the FF state. Recently, some experimental evidence has been reported in the heavy fermion superconductors [26] and ultracold Fermi gases [28]. However, there is still a lack of direct experimental evidence verifying the existence of FF state or LO state.

In the presence of both anisotropic SOC and effective Zeeman fields, recent theoretical studies revealed that the FF state with center-of-mass momentum perpendicular to the direction of the anisotropic SOC can be stabilized in a two-dimensional Fermi gas. A similar route to observe the FF phase in a three-dimensional Fermi gas was proposed [31, 32]. As is well known, by changing the single-particle dispersion, the SOC plays an important role in inducing the topological properties of the superfluid/superconducting system [2]. A natural question to ask is whether the FF state may be compatible with topological order. With the recent theoretical and experimental progress on SOC [20–22, 33], h_z can make the chemical potential fill the Fermi surface of a single helicity band, and h_x deforms the structure of the Fermi surface, so the topologically non-trivial FF state has been predicted in the continuous Fermi gas [34–37]. In contrast, when the Fermi energy level crosses both helicity bands simultaneously at half filling in the SOC lattice system [38], it is possible to contribute to the Cooper pair from two Fermi surfaces; in addition, it is significantly different from the results being obtained by the continuous model. Moreover, this kind of Cooper pair may drive the lattice system into the generalized LO state. For this instance, three questions can be posed. The first is whether the topological phase can persist into the LO phase; the second is, by tuning the chemical potential, can the tFF state emerge in the lattice system? The last is, do they support MFs?

In this article, we report the existence of the topological non-trivial LO phase with a nonzero integer Chern number $\mathcal{C} = 2$ (tLO_2) combining the topological non-trivial FF phase with $\mathcal{C} = -1$ (tFF_1) on the spin-orbit coupled lattice under Zeeman fields. Here, the Rashba SOC splits the single band into two helicity branches; in addition, Cooper pairs Δ_+ and Δ_- come from two helicity bands [see Fig. 1(a)]. When there is an in-plane Zeeman field h_x, the Cooper pairs from different bands have opposite center-of-mass momenta $\pm Q_y$ and different amplitudes ($\Delta_+ \neq \Delta_-$). Moreover, the competition between the Rashba SOC and Zeeman fields leads to the FF phase and the generalized LO phase without nodes [39]. On this basis, the out-of-plane Zeeman field h_z can drive the FF phase and the LO phase without nodes into the tFF_1 and tLO_2 phases for the over-doped and half-filled cases. Under half filling, $\mathcal{C} = 2$ becomes a characteristic property for the tSC states of the lattice-type model. In addition to the tFF_1 states with $\mathcal{C} = -1$

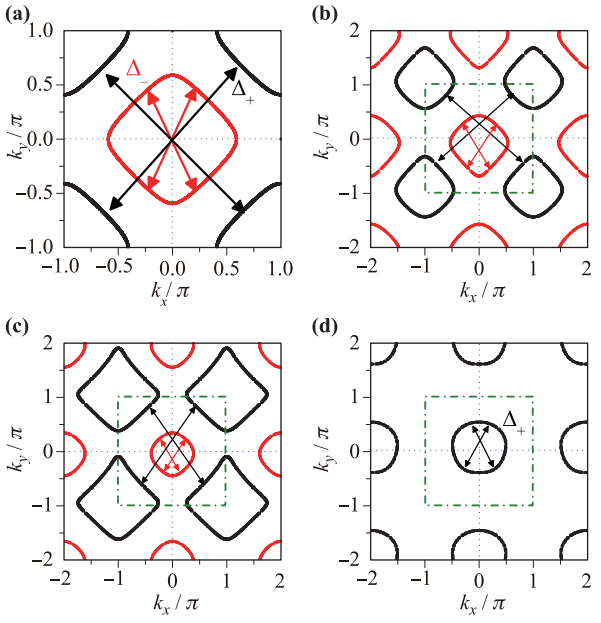

Fig. 1 Pairing mechanism on the Fermi surface for FF and LO states. **(a)** Intra-branch BCS pairing in two Fermi surfaces without Zeeman fields, **(b)** intra-branch pairing (the LO pairing) in two Fermi surfaces with Zeeman fields $h_z = h_x = 0.8$ for half filling, and **(c)** the doped case with Zeeman fields $h_z = 1.0$, $h_x = 0.5$, $\mu = -0.9$. **(d)** The case of (c), but with $\mu = -4.0$; here, only a single Fermi surface exists.

similar to the tFF with $\mathcal{C} = 1$ in the continuum Fermi gas [34, 35, 37], as a new quantum state of matter, the tLO_2 state, exhibiting the more stable inhomogeneous superfluid/superconducting order, provides a promising candidate for studying the topological properties of matter and searching for MFs. Of note is the fact that the tLO_1 state with $\mathcal{C} = 1$ can emerge in a small-parameter region of the doped phase diagram. To explore their topological properties, we also present the distribution of the lattice field strength for different Chern numbers, the edge states, and their local density of states (LDOS) spectra for inhomogeneous tSC states, which could be tested in future experiments.

Model Hamiltonian. Here we consider a minimal 2D lattice model with a Rashba SOC and both in-plane and out-of-plane Zeeman fields, which can be described by an effective Hamiltonian:

$$
\begin{aligned}
H &= H_{\mathrm{K}} + H_{\mathrm{R}} + H_{\Delta}, \\
H_{\mathrm{K}} &= -t \sum_{i,j,\sigma} \psi^{\dagger}_{i\sigma} \psi_{j\sigma} + \sum_{i,\sigma} (h_{\mathrm{z}} \sigma_z + h_{\mathrm{x}} \sigma_x - \mu) \psi^{\dagger}_{i\sigma} \psi_{i\sigma}, \\
H_{\mathrm{R}} &= \lambda \sum_{i} (\psi^{\dagger}_{i} \sigma_x \psi_{i+\hat{x}} + \psi^{\dagger}_{i} \sigma_y \psi_{i+\hat{y}} + \mathrm{h.c.}), \\
H_{\Delta} &= \sum_{i} (\Delta_i \psi^{\dagger}_{i\uparrow} \psi^{\dagger}_{i\downarrow} + \Delta^{*}_{i} \psi_{i\downarrow} \psi_{i\uparrow}),
\end{aligned}
\tag{1}
$$

where $\psi^{\dagger}_{i\sigma}$ ($\psi_{i\sigma}$) denotes the creation (annihilation) field operator of the fermionic particle with spin $\sigma \equiv (\uparrow, \downarrow)$ at site i, λ is the SOC strength, and h_x and h_z are the in-plane and out-of-plane Zeeman fields, respectively. The effective Hamiltonian can be achieved by solving the following Bogoliubov–de Gennes (BdG) equations:

$$\sum_j \begin{pmatrix} H_{ij\uparrow} & \lambda_1 & 0 & \Delta_{ij} \\ \lambda_2 & H_{ij\downarrow} & -\Delta_{ij} & 0 \\ 0 & -\Delta^*_{ij} & -H_{ij\uparrow} & \lambda_3 \\ \Delta^*_{ij} & 0 & \lambda_4 & -H_{ij\downarrow} \end{pmatrix} \begin{pmatrix} u^n_{j\uparrow} \\ u^n_{j\downarrow} \\ v^n_{j\uparrow} \\ v^n_{j\downarrow} \end{pmatrix} = \epsilon_n \begin{pmatrix} u^n_{i\uparrow} \\ u^n_{i\downarrow} \\ v^n_{i\uparrow} \\ v^n_{i\downarrow} \end{pmatrix}, \tag{2}$$

where $H_{ij\uparrow} = -t_{ij} - (\mu - h_z)\delta_{ij}$, $H_{ij\downarrow} = -t_{ij} - (\mu + h_z)\delta_{ij}$, $\lambda_m = \lambda\{[(-1)^{m+1}\delta_{i+e_x,j} + (-1)^m \delta_{i-e_x,j}] + \varepsilon_m[\mathrm{i}(\delta_{i+e_y,j} - \delta_{i-e_y,j})] - \varepsilon_m h_x \delta_{i,j}$ with $m = 1, 2$, $\varepsilon_m = -1$, and $m = 3, 4$, $\varepsilon_m = 1$. The SC pairing $\Delta_i = V\langle c_{i\uparrow} c_{i\downarrow}\rangle$ are determined self-consistently for a fixed chemical potential. In the following calculations, the energy is measured in units of the hopping integral t and $\lambda = 0.75$. We consider a very low temperature $T = 10^{-3}$ and the pairing interaction $V = 2.25$. Here, we assign different initial values of Δ_i using random numbers, and the calculation is repeated until the relative difference in the order parameter between two consecutive iteration steps is less than 10^{-5}. For multiple solutions, we compare their corresponding free energies to obtain the most energetically favored state.

To distinguish the FF and LO states, we define the amplitude variation of the order parameter $\sigma_1 = \sqrt{\sum_i (|\Delta_i| - \overline{|\Delta|})^2/N}$ with $\overline{|\Delta|} = \sum_i |\Delta_i|/N$ and phase variation $\sigma_2 = \sqrt{\sum_i |\Delta_i - \overline{\Delta}|^2/N}$ with $\overline{\Delta} = \sum_i \Delta_i/N$. The normal superfluid phase is characterized by $\overline{|\Delta|} \neq 0$, $\sigma_1 = \sigma_2 = 0$, $Q_y = 0$. For the LO phase $\overline{|\Delta|} \neq 0$, $\sigma_1 \neq 0$, $Q_y \neq 0$, whereas for the FF phase $\overline{|\Delta|} \neq 0$, $\sigma_1 = 0$, $\sigma_2 = \overline{|\Delta|}$, $Q_y \neq 0$ [39]. To describe the topological properties of the system, we calculated the Chern number in the hole branches $\mathcal{C} = \sum_l \mathcal{C}_l$. Here, by using the twisted boundary condition [40] because the system preserves the translational invariance of the system along the x direction, $\mathcal{C}_l = \frac{1}{2\pi}\int \mathrm{d}k_x \mathrm{d}\theta_y \Omega_l$ is the Chern number of the lth band. $\Omega_l = -2\mathrm{Im}\langle \frac{\partial \Psi_l}{\partial k_x} | \frac{\partial \Psi_l}{\partial \theta_y}\rangle$ is the Berry curvature [1], and $|\Psi_l\rangle$ is the eigenstate of the lth hole band of Eq. (2). For the 2D lattice model, $\mathcal{C}$ can be expressed as the sum of the lattice field strength: $\mathcal{C} = \sum_n \frac{\Omega_n}{2\pi}$.

Pairing mechanism and order parameter. To distinguish different roles for the SOC and the Zeeman field, we show the Fermi surface for SOC without Zeeman fields [see Fig. 1(a)]. Because of the SOC, the band of the system is split into upper and lower helicity branches, the Fermi surfaces of which are symmetric in the entire Brillouin zone (BZ). Pairing on different Fermi surfaces involves the BCS pairing mechanism between states of opposite momenta $\boldsymbol{k}$ and $-\boldsymbol{k}$. When applying in-plane and out-of-plane Zeeman fields [see Fig. 1(b)], two helicity Fermi surfaces become asymmetric along the y direction; the upper helicity Fermi surface moves along positive k_y, and the lower helicity Fermi surface moves along negative k_y. The asymmetric Fermi surface leads to a finite center-of-mass momentum $\pm Q_y$ of the superfluid/superconducting pairings, because the finite momentum Cooper pairs are LO states (with spatially varying order parameter amplitudes). Meanwhile, from the half filling in Fig. 1(b), we find that the upper-helicity and lower-helicity Fermi surfaces have the same size, implying that $\Delta_+ = \Delta_-$. As the system deviates from half filling [see Fig. 1(c)], the two helicity Fermi surfaces have different sizes, implying that $\Delta_+ \neq \Delta_-$. When the system corresponds to the over-doped case [see Fig. 1(d)], the lower helicity Fermi surface completely disappears, and the topology of the whole Fermi surface is completely changed. Because the contribution of the Cooper pairs comes only from an upper helicity Fermi surface, the system supports an FF state (only Δ_+).

To clarify the difference between the FF and LO states, Fig. 2 summarizes the detailed spatial profiles of the inhomogeneous tSC order parameters, such as the FF state with spatially uniform magnetization: m_x and m_z [see Fig. 2(a)], and the LO state with spatially oscillating magnetization, m_x and m_z [see Fig. 2(b)]. For the FF state, the pairing mainly comes from only one of the helicity Fermi surfaces, whereas for the LO state, the pairing comes from both helicity Fermi surfaces. As mentioned previously, compared with the traditional LO state, the real and imaginary parts of the order parameter in the tLO_2 phase stem from the relative phase arising from the superposition of Δ_+ and Δ_-, so Δ_i does not have nodes, and the system is gapped completely. Meanwhile, h_z drives the system from a non-topological to a topological phase, and we find that the Chern numbers are -1 for tFF_1 and 2 for tLO_2.

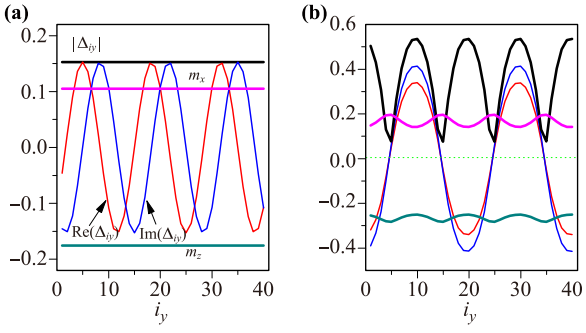

Fig. 2 Spatial profiles of order parameters for the tFF_1 and tLO_2 states: **(a)** the FF state order parameter, magnetization m_x along the x direction, and m_z along the z direction with $\mathcal{C} = -1$, $\mu = -2.95$, $h_x = 0.6$; **(b)** order parameter and magnetization for the LO state, $\mathcal{C} = 2$, $h_x = 0.6$, $h_z = 0.8$.

Global phase diagrams. The interplay among the in-plane and out-of-plane Zeeman fields, pairing, and SOC may result in distinct pairing states. To understand these phases better, the global phase diagram is present at half-filling on the $h_x - h_z$ plane (Fig. 3), and there are four different phases, including the conventional BCS state, the topological BCS state with $C = 2$, the LO phase, and the tLO_2 phase. It is well known that the conventional BCS state exists in a region with small h_x and h_z. For $h_z < 0.2$, with increasing h_x, the system is driven from the BCS phase into the generalized LO phase via a first-order transition; finally, h_x destroys the SC gap, and the system evolves into a normal metallic state. All these results are consistent with previous non-topological theoretical work. For $0.2 \leq h_z \leq 0.8$, the LO phase emerges in the large h_x region. In this region, the main change is that the BCS phase is initially driven into the tLO_2 phase by h_x and h_z, which is a new quantum state of matter. With increasing h_x, the tLO_2 phase transforms into the LO phase. For large $h_z \geq 0.8$, the phase structure becomes rich and the topological properties of the system are dominant. Besides the LO phase and the normal phase, there exists a topologically non-trivial tBCS_2 phase, despite the extremely small h_x. By turning up the strength of h_x, the tLO_2 phase emerges near the region of the tBCS_2 phase. As h_x further increases, the whole system is driven from the tLO_2 phase into the LO phase. Herein, this new tLO_2 phase can be simply considered the superposition of two effective p-wave pairings (tFF) in two helicity bands.

The μ–h_x-plane phase diagram is presented for a system far from half filling through chemical doping; see Fig. 4. In the region close to half filling, we obtain the tBCS_2 phase, the tLO_2 phase, and the LO phase, which is consistent with half filling. With decreasing μ, the topological properties of the tBCS_2 phase disappear, and the tBCS_2 phase evolves into a conventional BCS phase for small h_x; for moderate h_x, with decreasing chemical potential, the $\mathcal{C}$ of the tLO_2 phase changes from 2 to 1, and the system accordingly enters into the tLO_1 phase. From Fig. 6(a), the topological property of the tLO_1 phase principally comes from the contribution of the upper helicity Fermi surface including points of $k_x = \pi$. For large h_x, when the chemical potential is in the interval $-2.8 \leq \mu \leq 1$, distinguishing the FF and LO phases is difficult because the two are very close, so they are collectively called the FFLO phase. When the system is far from half filling $\mu \leq -2.8$, there exists only one helicity Fermi surface. In this circumstance, the tBCS_1 phase emerges for small h_x. With increasing h_x, the tBCS_1 phase evolves to the tFF_1 phase within the FF phase. Here, $\mathcal{C}$ comes from the contribution of the upper helicity Fermi surface for both tLO_1 and tFF_1 phases. Although the upper helicity Fermi surface contributes to the Chern numbers of the tLO_1 and tFF_1 phases, the topology of their Fermi surfaces is completely different, corresponding to different levels of chemical doping, as seen in Figs. 1(c) and (d).

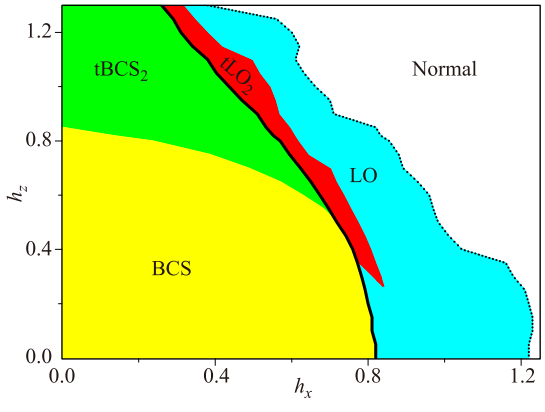

Fig. 3 Phase diagram of the FFLO superfluid for half-filling. Color identifies the different phases. The superfluid has topological superfluid/superconducting phases with $\mathcal{C} = -1$ (tBCS_1) and $\mathcal{C} = 2$ (tBCS_2), a LO phase with $C = 2$ (tLO_2), a generalized topological trivial LO phase (LO), and a normal phase. Above the dotted line, the order parameter is less than 0.001, corresponding to the normal phase. The solid black line corresponds to the first-order phase transition boundary. Here, we choose $\mu = 0.0$.

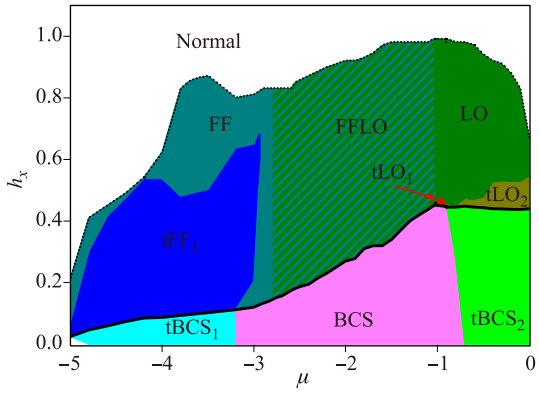

Fig. 4 Phase diagram of a doped FFLO superfluid. The different phases are labeled with different colors. Compared with half filling, the additional phases are the LO phase with $\mathcal{C} = 1$ (tLO_1) and the FF phase with $\mathcal{C} = -1$ (tFF_1). The solid and dotted lines have the same significance as in Fig. 3. Here, we choose $h_z = 1.0$.

Evolution of minimal excitation gap and Chern number. The band inversion is an important feature of the emergence of a topological quantum transition, and this inversion corresponds to closing and reopening the minimal excitation gap E_g. To understand the topological transition better, we present the evolution of a minimal excitation gap E_g across the topological

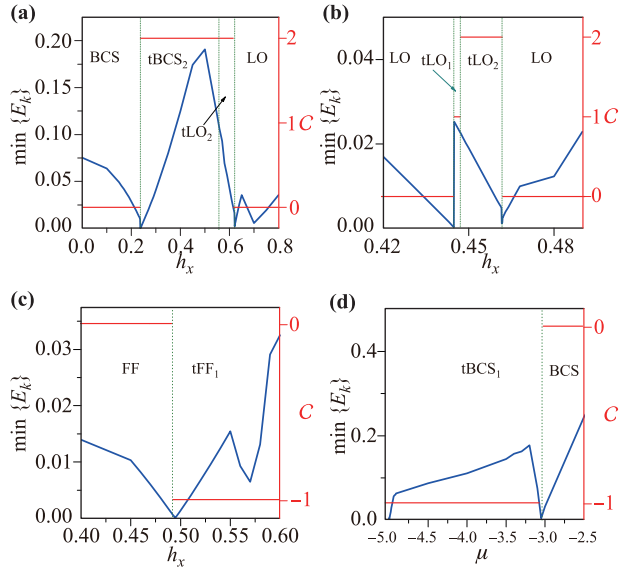

Fig. 5 Evolution of minimal excitation gap of inhomogeneous tSC states. Evolution of the minimal excitation gap across the topological phase boundary with h_x in (a), (b), and (c); in (d), the topological phase transition emerges with increasing chemical potential. The red line presents the Chern number. When increasing h_x and μ, at the topological phase boundary, the excitation closes and reopens. In **(a)**, $\mu = 0$, $h_z = 0.8$; **(b)**, $\mu = -0.9$, $h_z = 1$; **(c)**, $\mu = -2.95$, $h_z = 1$; **(d)**, $h_z = 1$, $h_x = 0$.

phase boundary with h_z and μ in Fig. 5. For a fixed out-of-plane Zeeman field $h_z = 0.8$ such as in Fig. 5(a), with increasing h_x, at a fixed point of h_x, E_g first closes and reopens, marking the transition from the BCS phase into the tBCS_2 phase, and the Chern number changes from 0 to 2, accordingly. With a further increase in h_x, the tBCS_2 phase turns into the tLO_2 phase. With a continued increase in h_x, at the second fixed point of h_x, E_g closes and reopens again, and the Chern number changes from 2 to 0, accordingly, marking the transition from the tLO_2 phase into the LO phase. For $h_z = 1$ and $\mu = -0.9$ [Fig. 5(b)], because h_z is stronger, the system first presents the LO phase, and then transforms into the tLO_1 phase ($\mathcal{C} = 1$) with increasing h_x. At the transition point, we detect a closing and reopening of E_g. At the same time, the Chern number becomes 2. Nevertheless, this tLO_1 phase extends over a small domain and with increasing h_x, it quickly enters into the tLO_2 phase. With stronger h_x, the order parameter begins to become progressively smaller, and increasing numbers of nodes begin to emerge. These nodes destroy the topological properties of the system and drive the system from the tLO_2 into the LO phase again. For a sufficiently low band filling [Fig. 5(c)], we can obtain further access to the FF phase, when h_x is increased; the FF phase transforms into the tFF_1 with $\mathcal{C} = -1$. Overall, for a sufficiently strong h_x, the system finally enters the normal phase. In addition to h_x, by tuning down band filling [see Fig. 5(d)], a topological phase transition also emerges between the BCS and tBCS_1 phases. We summarize these results by concluding that changes in h_x and adjustments of μ yield a variety of different topological phases for the system.

To clearly show the origin of the Chern number in these tSC states, we calculated the lattice field strength of the Chern number (see Fig. 6). For the tBCS_1 state in Fig. 6(a), we see that both peak streaks in field strength point upwards and combine constructively with the positive background, to contribute to a nonzero Chern number 1. In contrast, a downward-pointing peak streak arises around $k_x = 0$ and does not contribute to a nonzero Chern number because it opposes the positive background. For the tBCS_2 and tLO_2 states of Figs. 6(b) and (c), three positive-peak streaks in the lattice field strength point upwards and combine constructively. Hence, the non-zero Chern number is determined by both the non-trivial points around $k_x = 0$ and $k_x = \pi$, which belong to the high and low helicity Fermi surfaces, respectively. Compared with the tBCS_2 and tLO_2 states, the main contribution of $\mathcal{C}$ for the tBCS_1 and tFF_1 states comes from three streaks of negative peaks near $k_x = 0$, which means $\mathcal{C} = -1$ is determined by the non-trivial points near $k_x = 0$, belonging to only one helicity Fermi surface. Clearly, the value of $\mathcal{C}$ is closely related to the topological structure of the two helicity Fermi surfaces.

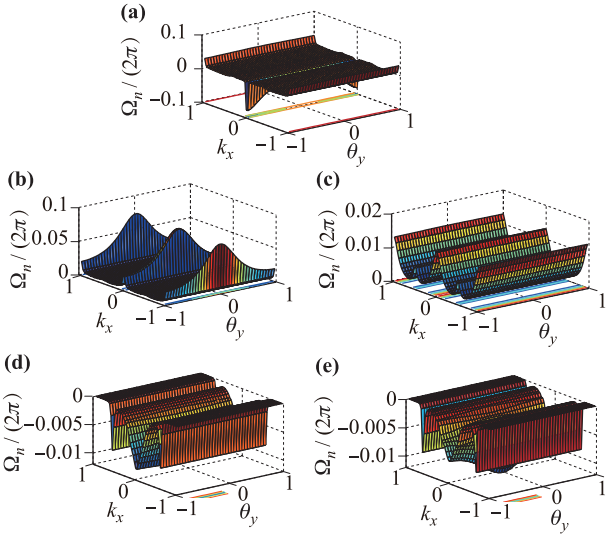

Fig. 6 Lattice field strength of the Chern numbers for the inhomogeneous tSC states. Berry curvature of the tLO_1 state with $\mathcal{C} = 1$, $\mu = -0.93$, $h_x = 0.47$ for **(a)**; **(b)** the tBCS_2 state with $\mathcal{C} = 2$, $h_z = 0.8$, $h_x = 0.3$; **(c)** the tLO_2 state with $\mathcal{C} = 2$, $h_z = 0.8$, $h_x = 0.6$; **(d)** the tBCS_1 state with $\mathcal{C} = -1$, $\mu = -3.2$, $h_x = 0.1$; **(e)** the tFF_1 state with $\mathcal{C} = -1$, $\mu = -2.95$, $h_x = 0.6$.

We know the two topological points $k_x = 0$ and $k_x = \pi$ will be highly critical in the lattice system, as reflected by the edge states in Fig. 7. In these edge states, gapless edge modes arise at either $k_x = 0$, $k_x = \pi$, or two simultaneous points in pairs. Hence the value of $\mathcal{C}$ depends on comprehensive effects of the special structure of the two helicity Fermi surfaces at the half-filling and doping level.

Edge state and the LDOS. For the tFF($\mathcal{C} = 1$) state, the preceding theoretical work shows support for exotic chiral edge modes [34, 35, 37]. In this work, we looked into the question of whether the $tLO_{1,2}$ and tFF_1 states support exotic chiral edge modes. To understand the topological property of the $tLO_{1,2}$ and tFF_1 states more clearly, we consider a 2D strip, the lattice size of which has width $x = 40$ and length $y = 100$. Because the state obeys translation invariance along the x-direction, we adopt periodic and open boundary conditions along the x- and y-directions, respectively, with k_x as a good quantum number. The energy spectrum and the LDOS are plotted in Fig. 7. There exists a distinct energy gap because of the SOC, and gapless edge states appear at $k = 0$ and $k = \pi$; see Fig. 7(a). For the tFF_1 state, a gapless edge state appears only at $k = 0$ [Fig. 7(c)], and only at $k = \pi$ for the tLO_1 state [Fig. 7(e)]. The presence of edge states indicates topological properties for both the $tLO_{1,2}$ and tFF_1 states in momentum space. In real space, we calculated the LDOS spectra at $\omega = 0$ along the lattice i_y in Figs. 7(b), (d), and (f). At the edge of the lattice system, we find two zero-energy modes, which implies that the tLO_2 and tFF_1 states support two local MFs at two edges of the strip. For the tLO_1 state, the gap protecting the edge state is quite narrow, and the scattering strength from the edge becomes relatively strong, which leads to the formation of the Mott insulating gap at the edge of the strip. The Cooper pairs in bulk bounce off from the Mott insulating gap and form a new edge state in the new location. This results in migration of the edge state towards the center of the bulk. Thus, we find that the edge state of the tLO_1 is not exactly at the two edges of the strip, but near the center of the bulk [Fig. 7(f)].

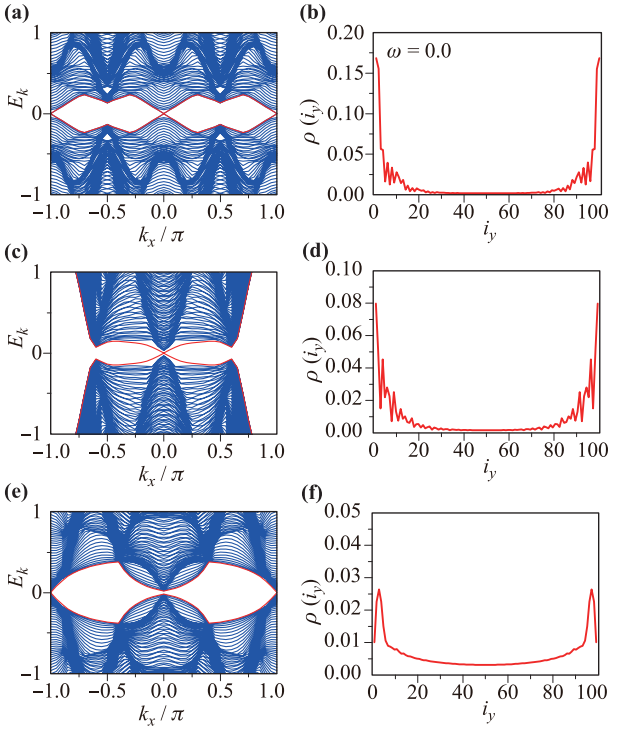

Fig. 7 Edge states and local density of states for tLO_2, tFF_1, and tLO_1 phases in a 2D strip: **(a)** the edge state of the tLO_2 with $C = 2$, $h_z = 0.8$ $h_x = 0.6$; **(b)** the local density of states for the tLO_2 state at zero energy, with the same parameters as those in (a); **(c)** the edge state of the tFF_1 with $C = -1$, $\mu = -3$, $h_x = 0.4$; **(d)** the local density of states for the tFF_1 state, with the parameters as those in (c); **(e)** the edge state of the tLO_1 with $C = 1$, $\mu = -0.93$, $h_x = 0.47$, $h_z = 1.0$; **(f)** the local density of states for the tLO_1 state, with the parameters as those in (e).

Our proposed tLO_2 and tFF_1 phases may also be realized in a spin-orbit coupled lattice system of semiconductor/superconductor heterostructures or cold atom gas [15, 16]. In particular, for cold-atom systems, some promising theoretical proposals to generate Rashba-type SOCs have already been proposed [33], and the effective Zeeman field and SOC have been realized experimentally by two-photon detuning and modulated Raman fields [20–22]. All this theoretical and experimental progress has laid a solid foundation to achieve inhomogeneous tSC states. Our numerical results are rather different from the results using a continuum model, and the lattice structure plays an important role in obtaining and stabilizing these exotic quantum states, especially the LO and tLO_2 states, which appear more stable. As a first attempt, we predict new quantum states — the tFF_1 state and the $tLO_{1,2}$ state — under the present lattice model, and their emergence also uncovers a novel mechanism for inhomogeneous tSC states in two spin-mixed asymmetric helicity bands of the SOC system. Compared with the topological trivial FFLO states, the topological FFLO states might be realized in experiments more easily through topological protection.

In summary, we propose that tFF_1 and $tLO_{1,2}$ states with finite momentum pairings can be realized using the SOC lattice under Zeeman fields with s-wave pairing. A global phase diagram has been presented, which includes different topological phases in the given parameter region. We also explored the detailed structures of the inhomogeneous order parameters, the distribution of the lattice field strength for different Chern numbers, the edge states of the tSC phases, and LDOSs. The tLO_2

state is identified for the first time in the SOC lattice under Zeeman fields and combines with the tFF_1 state to broaden and deepen our understanding of topological superfluids.

Acknowledgements We thank Y. S. Wu, R. B. Tao, T. K. Lee, and A. Varlamov for fruitful discussions. This work was supported by the State Key Programs of China (Grant Nos. 2017YFA0304204, and 2016YFA0300504) and the National Natural Science Foundation of China (Grant Nos. 11625416 and 11474064).

References

1. D. Xiao, M. C. Chang, and Q. Niu, Berry phases effects on electronic properties, *Rev. Mod. Phys.* 82(3), 1959 (2010)
2. X. L. Qi and S. C. Zhang, Topological insulators and superconductors, *Rev. Mod. Phys.* 83(4), 1057 (2011)
3. E. Majorana, Teoria simmetrica dell'elettrone e del positrone, *Nuovo Cim.* 14(4), 171 (1937)
4. F. Wilczek, Majorana returns, *Nat. Phys.* 5(9), 614 (2009)
5. C. Nayak, S. H. Simon, A. Stern, M. Freedman, and S. Das Sarma, Non-Abelian anyons and topological quantum computation, *Rev. Mod. Phys.* 80(3), 1083 (2008)
6. L. P. Rokhinson, X. Liu, and J. K. Furdyna, The fractional a.c. Josephson effect in a semiconductor-superconductor nanowire as a signature of Majorana particles, *Nat. Phys.* 8(11), 795 (2012)
7. A. Das, Y. Ronen, Y. Most, Y. Oreg, M. Heiblum, and H. Shtrikman, Zero-bias peaks and splitting in an Al-InAs nanowire topological superconductor as a signature of Majorana fermions, *Nat. Phys.* 8(12), 887 (2012)
8. M. T. Deng, C. L. Yu, G. Y. Huang, M. Larsson, P. Caroff, and H. Q. Xu, Anomalous zero-bias conductance peak in a Nb-InSb nanowire-Nb hybrid device, *Nano Lett.* 12(12), 6414 (2012)
9. V. Mourik, K. Zuo, S. M. Frolov, S. R. Plissard, E. P. A. M. Bakkers, and L. P. Kouwenhoven, Signatures of Majorana fermions in hybrid superconductor-semiconductor nanowire devices, *Science* 336(6084), 1003 (2012)
10. L. Mao, M. Gong, E. Dumitrescu, S. Tewari, and C. Zhang, Hole-doped semiconductor nanowire on top of an *s*-wave superconductor: a new and experimentally accessible system for Majorana fermions, *Phys. Rev. Lett.* 108(17), 177001 (2012)
11. G. Moore and N. Read, Nonabelions in the fractional quantum hall effect, *Nucl. Phys. B* 360(2–3), 362 (1991)
12. A. P. Mackenzie and Y. Maeno, The superconductivity of Sr_2RuO_4 and the physics of spin-triplet pairing, *Rev. Mod. Phys.* 75(2), 657 (2003)
13. N. Read and D. Green, Paired states of fermions in two dimensions with breaking of parity and time-reversal symmetries and the fractional quantum Hall effect, *Phys. Rev. B* 61(15), 10267 (2000)
14. L. Fu and C. L. Kane, Superconducting proximity effect and Majorana fermions at the surface of a topological insulator, *Phys. Rev. Lett.* 100(9), 096407 (2008)
15. J. D. Sau, R. M. Lutchyn, S. Tewari, and S. Das Sarma, Generic new platform for topological quantum computation using semiconductor heterostructures, *Phys. Rev. Lett.* 104(4), 040502 (2010)
16. R. M. Lutchyn, J. D. Sau, and S. Das Sarma, Majorana fermions and a topological phase transition in semiconductor-superconductor heterostructures, *Phys. Rev. Lett.* 105(7), 077001 (2010)
17. Y. Oreg, G. Refael, and F. von Oppen, Helical liquids and Majorana bound states in quantum wires, *Phys. Rev. Lett.* 105(17), 177002 (2010)
18. J. Alicea, Y. Oreg, G. Refael, F. von Oppen, and M. P. A. Fisher, Non-Abelian statistics and topological quantum information processing in 1D wire networks, *Nat. Phys.* 7(5), 412 (2011)
19. A. C. Potter and P. A. Lee, Multichannel generalization of Kitaev's Majorana end states and a practical route to realize them in thin films, *Phys. Rev. Lett.* 105(22), 227003 (2010)
20. Y. J. Lin, K. Jiménez-García, and I. B. Spielman, Spin–orbit-coupled Bose–Einstein condensates, *Nature* 471(7336), 83 (2011)
21. P. Wang, Z.Q. Yu, Z. Fu, J. Miao, L. Huang, S. Chai, H. Zhai, and J. Zhang, Spin–orbit coupled degenerate Fermi gases, *Phys. Rev. Lett.* 109(9), 095301 (2012)
22. L. W. Cheuk, A. T. Sommer, Z. Hadzibabic, T. Yefsah, W. S. Bakr, and M. W. Zwierlein, Spin-injection spectroscopy of a spin-orbit coupled Fermi gas, *Phys. Rev. Lett.* 109(9), 095302 (2012)
23. M. Sato, Y. Takahashi, and S. Fujimoto, Non-Abelian topological order in *s*-wave superfluids of ultracold fermionic atoms, *Phys. Rev. Lett.* 103(2), 020401 (2009)
24. X.-J. Liu, H. Pu, and H. Hu, Probing Majorana fermions in spin-orbit-coupled atomic Fermi gases, *Phys. Rev. A* 85, 021603(R) (2011)
25. R. Casalbuoni and G. Nardulli, Inhomogeneous superconductivity in condensed matter and QCD, *Rev. Mod. Phys.* 76(1), 263 (2004)
26. M. Kenzelmann, T. Strassle, C. Niedermayer, M. Sigrist, B. Padmanabhan, M. Zolliker, A. D. Bianchi, R. Movshovich, E. D. Bauer, J. L. Sarrao, and J. D. Thompson, Coupled superconducting and magnetic order in $CeCoIn_5$, *Science* 321(5896), 1652 (2008)
27. L. Li, C. Richter, J. Mannhart, and R. C. Ashoori, Coexistence of magnetic order and two-dimensional superconductivity at $LaAlO_3/SrTiO_3$ interfaces, *Nat. Phys.* 7(10), 762 (2011)

28. Y. A. Liao, A. S. C. Rittner, T. Paprotta, W. Li, G. B. Partridge, R. G. Hulet, S. K. Baur, and E. J. Mueller, Spin-imbalance in a one-dimensional Fermi gas, *Nature* 467(7315), 567 (2010)
29. P. Fulde and R. A. Ferrell, Superconductivity in a strong spin-exchange field, *Phys. Rev.* 135(3A), A550 (1964)
30. A. I. Larkin and Y. N. Ovchinnikov, Nonuniform state of superconductors, *Zh. Eksp. Teor. Fiz.* 47, 1136 (1964)
31. F. Wu, G. Guo, W. Zhang, and W. Yi, Unconventional superfluid in a two-dimensional Fermi gas with anisotropic spin-orbit coupling and Zeeman fields, *Phys. Rev. Lett.* 110(11), 110401 (2013)
32. Z. Zheng, M. Gong, X. Zou, C. Zhang, and G. Guo, Route to observable Fulde–Ferrell–Larkin–Ovchinnikov phases in three-dimensional spin-orbit-coupled degenerate Fermi gases, *Phys. Rev. A* 87, 031602(R) (2013)
33. X. J. Liu, K. T. Law, and T. K. Ng, Realization of 2D spin-orbit interaction and exotic topological orders in cold atoms, *Phys. Rev. Lett.* 112(8), 086401 (2014)
34. C. Qu, Z. Zheng, M. Gong, Y. Xu, L. Mao, X. Zou, G. Guo, and C. Zhang, Topological superfluids with finite momentum pairing and Majorana fermions, *Nat. Commun.* 4, 2710 (2013)
35. W. Zhang and W. Yi, Topological Fulde–Ferrell–Larkin–Ovchinnikov states in spin-orbit-coupled Fermi gases, *Nat. Commun.* 4, 2711 (2013)
36. C. Chen, Inhomogeneous topological superfluidity in one-dimensional spin-orbit-coupled Fermi gases, *Phys. Rev. Lett.* 111(23), 235302 (2013)
37. Y. Cao, S.H. Zou, X.J. Liu, S. Yi, G.L. Long, and H. Hu, Gapless topological Fulde–Ferrell superfluidity in spin-orbital coupled Fermi gases, *Phys. Rev. Lett.* 113(11), 115302 (2014)
38. T. Zhou, Y. Gao, and Z. D. Wang, Topological quantum phase transitions and edge states in spin-orbital coupled Fermi gases, *Sci. Rep.* 4(1), 5218 (2015)
39. Y. Xu, C. Qu, M. Gong, and C. Zhang, Competing superfluid orders in spin-orbit coupled fermionic cold atom optical lattices, *Phys. Rev. A* 89(1), 013607 (2014)
40. D. N. Sheng, Z. Y. Weng, L. Sheng, and F. D. M. Haldane, Quantum spin-Hall effect and topologically invariant Chern numbers, *Phys. Rev. Lett.* 97(3), 036808 (2006)